crystals

MDPI

Article

Lithium Niobate Thin Film on Silicon Fabricated by Pulsed Laser Deposition

Shaoqing Song †, Tianqi Xiao †, Jiashun Song, Hongde Liu *, Dahuai Zheng *, Yongfa Kong * and Jingjun Xu

MOE Key Laboratory of Weak-Light Nonlinear Photonics, School of Physics and TEDA Institute of Applied Physics, Nankai University, Tianjin 300071, China; 1410228@mail.nankai.edu.cn (S.S.); tq_xiao@163.com (T.X.); nku2023song@163.com (J.S.); jjxu@nankai.edu.cn (J.X.)

* Correspondence: liuhd97@nankai.edu.cn (H.L.); dhzheng@nankai.edu.cn (D.Z.); kongyf@nankai.edu.cn (Y.K.)

† These authors contributed equally to this work.

Abstract

Lithium niobate ($LiNbO_3$, LN) is a multifunctional material with broad applicability in photonic and electronic devices. Recent advances in lithium niobate on insulator (LNOI) technology have significantly enhanced the integration density and miniaturization potential of LN-based platforms. Among the various fabrication techniques available, pulsed laser deposition (PLD) presents a cost-effective and versatile alternative to crystalline ion slicing (CIS), particularly advantageous for achieving high doping concentrations. However, a persistent challenge in PLD-grown lithium niobate film is cracking, primarily induced by the substantial thermal stress resulting from the mismatch in thermal expansion coefficients between LN and the substrate. In this study, we implemented a series of process modifications to address the cracking issue and successfully achieved crack-free LN films by introducing a lithium-deficient phase. This approach enabled the successful fabrication of highly Fe^{3+}-doped LN films with a high electrical conductivity of 9.95×10^{-5} S/m while also exhibiting characteristic polarization switching behavior. These results demonstrate that PLD enables the fabrication of highly doped, structurally robust LN films and holds significant potential for the development of advanced electronic and optoelectronic devices.

Keywords: lithium niobate thin film; pulsed laser deposition; crack-free; LNOI

check for updates

Academic Editor: Alla S. Sologubenko

Received: 28 July 2025
Revised: 20 August 2025
Accepted: 25 August 2025
Published: 27 August 2025

Citation: Song, S.; Xiao, T.; Song, J.; Liu, H.; Zheng, D.; Kong, Y.; Xu, J. Lithium Niobate Thin Film on Silicon Fabricated by Pulsed Laser Deposition. *Crystals* **2025**, *15*, 756. https://doi.org/10.3390/cryst15090756

Copyright: © 2025 by the authors. Licensee MDPI, Basel, Switzerland. This article is an open access article distributed under the terms and conditions of the Creative Commons Attribution (CC BY) license (https://creativecommons.org/licenses/by/4.0/).

1. Introduction

Lithium niobate ($LiNbO_3$, LN) is a highly promising material for integrated photonic applications due to its exceptional optical and electro-optical properties. It features a broad transparency window, a high refractive index (n_o = 2.21, n_e = 2.14 at 1550 nm), and pronounced second-order nonlinear optical and electro-optic coefficients [1–3]. In addition, LN exhibits ferroelectric, piezoelectric, and thermo-optic effects, further enhancing its versatility [4–6].

Recent advances in fabrication techniques, such as precision polishing and crystal ion slicing (CIS), have enabled the production of thin-film lithium niobate (TFLN) with well-controlled thicknesses [7]. These thin films can be bonded onto insulators with lower refractive indices (e.g., silicon dioxide), thereby forming lithium niobate on insulator (LNOI) structures analogous to the widely used silicon-on-insulator (SOI) platform [8]. Leveraging mature micro- and nanofabrication technologies [9], LNOI-based photonic devices have undergone rapid development in recent years. A wide range of high-performance device architectures has been demonstrated for various applications, including electro-optic

modulators [10,11], acousto-optic modulators [12,13], optical frequency combs [14,15], nonlinear wavelength converters [16,17], and sources of entangled photon pairs [18,19]. These advancements signify the emergence of a new era in lithium niobate photonics.

Although CIS is currently the predominant technique for the fabrication of LNOI structures—owing to the persistent quality and reproducibility challenges associated with heterogeneous epitaxial growth on insulator substrates [20]—this method presents several inherent limitations. Specifically, CIS-based LNOI fabrication relies on bulk LN crystals, which hinders the achievement of high doping concentrations or spatially localized doping and increases susceptibility to elemental segregation during processing [21,22]. Furthermore, the implantation of He^+ ions during the CIS process adversely affects the structural integrity and functional performance of the LN layer.

Pulsed laser deposition (PLD) has emerged as a promising alternative method for LNOI fabrication, offering the advantage of achieving higher doping concentrations [23–27]. PLD is suitable for complex oxides since it has the ability to preserve the stoichiometric composition of the target. Notably, the fabrication of LN–silicon oxide composite micro-disks resonators via PLD highlights the method's potential for LN photonics applications [28]. PLD offers several unique advantages for LN film growth on silicon substrates. Unlike CIS, which requires bulk LN crystals and is limited in doping flexibility, PLD enables controlled high-concentration doping and spatially selective modification. However, LN films deposited on silicon substrates via PLD exhibit cracking. This phenomenon arises from the mismatch in thermal expansion coefficients between LN and silicon. LN exhibits anisotropic thermal expansion—19.2 $\times$ 10^{-6} K^{-1} along the (1120) plane and 2.7 $\times$ 10^{-6} K^{-1} along the (0006) plane at 25 °C, compared to silicon (2.6 $\times$ 10^{-6} K^{-1}) and silicon oxide (0.5 $\times$ 10^{-6} K^{-1}) [29,30]. Thermal stress induces film cracking, hindering the fabrication of LNOI photonic devices.

In this study, we report a fabrication process for the growth of LN films on silicon substrates using PLD. We successfully fabricated LN films doped with high concentrations of Er^{3+} and Fe^{3+}. All samples exhibited a preferred <006> orientation, indicating c-axis alignment within the lithium niobate crystal structure. To address the persistent issue of film cracking, we employed a lithium-deficient composition strategy. The microstructural characteristics and electrical properties of the films were systematically investigated using a range of characterization techniques. This approach effectively mitigated crack formation and significantly enhanced the electrical conductivity of the highly Fe^{3+}-doped LN films. PLD enables the localized doping of LNOI structures with greater ease [31] and facilitates the development of three-dimensional (3D) LNOI device architectures [32,33].

2. Materials and Methods

The LN films were deposited on Si substrates using PLD. A KrF excimer laser (λ = 248 nm, pulse duration τ = 25 ns) served as the light source, with the laser beam incident at a 45° angle relative to the target. Prior to deposition, the vacuum chamber was evacuated to a base pressure of 10^{-6} Pa. After deposition, the samples were in situ annealed at the growth temperature for 60 min. The temperature was then programmed to decrease to approximately 100 °C, after which the samples were allowed to cool naturally to room temperature. The target-to-substrate distance was maintained at 40 mm. The deposition parameters for all samples are listed in Table 1. The vacuum chamber of the PLD system was supplied by SKY Technology Development Co., Ltd. CAS, (Shenyang, China) and the laser source was a COMPEX PRO 205 F from Coherent (Santa Clara, CA, USA).

Film morphology and microstructure were characterized by X-ray diffraction (XRD), optical microscopy, and scanning electron microscopy (SEM). θ–2θ XRD scans were performed using a Bruker D8 ADVANCE diffractometer (Bruker, Karlsruhe, Germany). Optical

images were acquired using a charge-coupled device (CCD) camera, and SEM characterization was conducted using a Helios Nanolab^{TM} 600i (FEI Company, Hillsboro, OR, USA). Atomic force microscopy (AFM) and piezoresponse force microscopy (PFM) measurements were carried out using an MFP-3D Origin system (Oxford Instruments, Abingdon, England). Current–voltage (I-U) characteristics were measured using an FS-Pro Semiconductor Parameter Test System (Primarius Technologies Co., Ltd., Shanghai, China). Gold electrodes (500 μm in diameter) were deposited via PLD to serve as the top contact for electrical measurements.

Table 1. Detailed parameters of samples. Target details: A, a 2.0 mol% erbium-doped congruent lithium niobate (CLN) wafer grown by the Czochralski method; B, a lithium-rich (80%) lithium niobate ($LiNbO_3$, LN) ceramic prepared by solid-state synthesis; C, a 5.0 mol% erbium-doped CLN ceramic prepared by solid-state synthesis; and D, a 5.0 mol% iron-doped LN ceramic obtained from ZHONGNUO ADVANCED MATERIAL (BEIJING) TECHNOLOGY CO., LIMITED (Beijing, China). Targets A, B, and C were fabricated in our laboratory. The fabrication procedure of B and C comprised an initial sintering of the powder, followed by binder addition, compaction by pressing, and a secondary sintering step.

Sample	Substrate Material	Target	Substrate Temperature (°C)	Programmed Cooling Time (h)	Laser Repetition Frequency (Hz)	Energy Density (J/cm^2)	Deposited Time (min)	Oxygen Pressure (Pa)
a	Si <111>	A	750	—	1	2.1	60	30
b	Si <100>	A	750	6	1	2.1	60	30
c	Si <111>	B	750	15	1	2.1	60	30
d	Si <111>	B	750	15	3	2.1	20	30
e	Si <111>	B	750	30	1	2.1	60	20
f	Si <100>	C	750	5	3	1.35	20	20
g	Si <100>	D	750	5	3	1.35	20	20
h	Si <100>	D	650	4	3	1.35	20	20
i	Si <100>	D	600	3.75	3	1.35	20	20

3. Results and Discussion

3.1. Strategies for Crack Suppression in LN Films

To explore the optimal conditions for the growth of LN film on Si substrates, a series of samples were fabricated. Samples a and b were deposited using Target A, with a laser repetition rate of 1 Hz and a deposition duration of 60 min. Sample a was grown on a Si <111> substrate and cooled naturally to room temperature, while sample b was grown on a Si <100> substrate and subjected to a programmed cooling of 6 h. Er doping imparts luminescent characteristics to LN. The XRD patterns of both samples, along with the corresponding PDF cards for $LiNbO_3$ and Si, are shown in Figure 1a. Both samples exhibit a prominent LN diffraction peak at 39.1°, corresponding to the <006> orientation. Additionally, a secondary peak at 38.3°, corresponding to the <-602> orientation of the $LiNb_3O_8$ phase, is observed in both samples. The presence of this peak suggests partial lithium volatilization during film growth. The XRD patterns for LN films grown on Si <111> and Si <100> substrates are nearly identical, indicating that Si substrate orientation has a negligible impact on the film phase under the growth conditions we employed. The thermal expansion coefficient of silicon is isotropic; therefore, changing the substrate orientation does not alter the thermal expansion mismatch. Consequently, both substrate orientations exhibit noticeable cracking in the thin-film optical mirrors.

To suppress the formation of lithium-deficient phases, a lithium-rich target (Target B) was employed for the growth of samples c–e on Si <111> substrates. As lithium-rich LN crystals could not be successfully grown, ceramic targets were employed instead. The cooling and annealing durations were extended, with a programmed cooling time of 15 h

applied to samples c and d. As shown in Figure 1a, films deposited with the lithium-rich target exhibit a strong <006> orientation without peaks corresponding to lithium-deficient phases. Surface analysis of sample c via SEM (Figure 1d) reveals the presence of fine surface cracks and a relatively high density of large particulates. To reduce particle contamination, the laser repetition frequency was increased to 3 Hz for sample d, which led to a noticeable decrease in surface particle density. However, substantial cracking persisted, as shown in Figure 1e. To further investigate the effect of oxygen pressure on cracking, the oxygen partial pressure was reduced to 20 Pa during the deposition of sample e. Nonetheless, this adjustment did not eliminate film cracking.

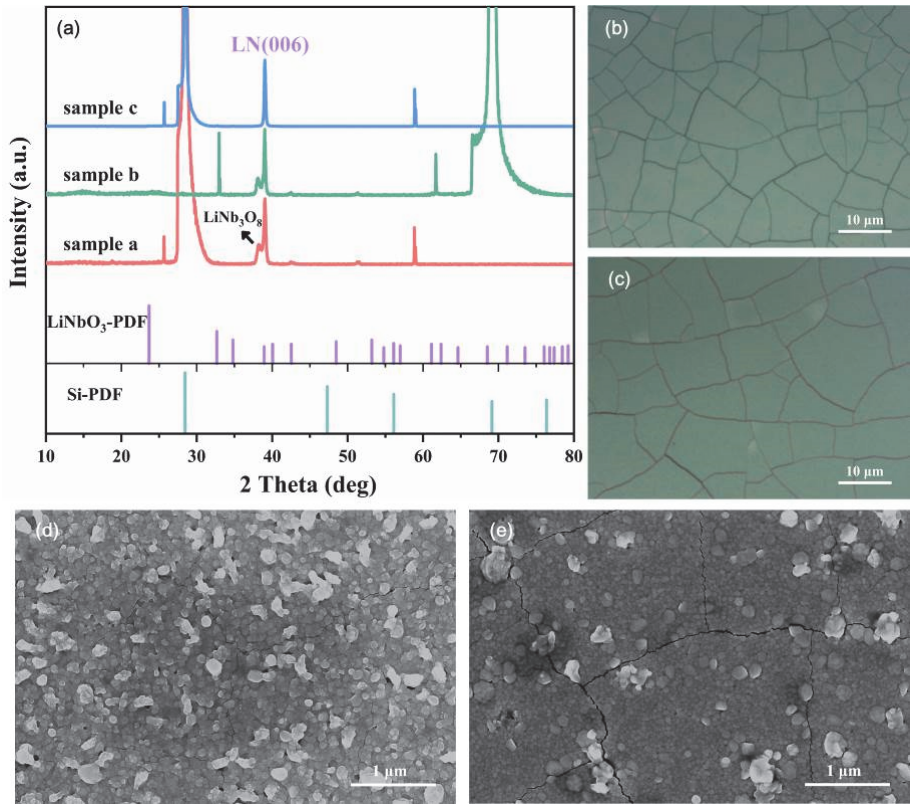


Figure 1. (**a**) X-ray diffraction (XRD) patterns of samples a–c in the 2θ range of 10–80°, compared with reference diffraction patterns of $LiNbO_3$ (ICDD PDF #20-0631) and Si (ICDD PDF #27-1402). The peaks at 33° for sample b originated from the Si <100> oxide layer; optical micrographs of (**b**) sample a and (**c**) sample b captured by charge-coupled device (CCD) imaging; scanning electron microscopy (SEM) micrographs of (**d**) sample c and (**e**) sample d.

As LN films prepared with lithium-rich targets consistently exhibit cracking, we explored adjusting the components to mitigate this problem. To reduce the presence of large surface particles and thereby lower surface roughness, the laser energy was slightly decreased during deposition. The XRD pattern of sample f, shown in Figure 2a, exhibits a prominent peak at 39.1°, corresponding to the <006> orientation of $LiNbO_3$, and an additional peak at 38.1°, attributed to the <-602> orientation of the $LiNb_3O_8$ phase [28]. As shown in Figure 2b, sample f displays a surface without visible cracks. These results suggest that the controlled introduction of lithium-deficient phases may play a critical role in suppressing crack formation in LN films. To further verify this hypothesis, sample g was prepared under identical conditions using an iron-doped target (Target D). LN optical devices are significantly influenced by the presence of lithium-deficient phases; therefore, LN films exhibiting such phases are more suitable for electrical applications. Furthermore, Fe doping can enhance the electrical properties of LN films. The XRD pattern and optical

microscopy image of sample g are presented in Figure 2c,d, respectively. Sample g shows a clear <006> orientation and the presence of a lithium-deficient phase, along with a smooth, crack-free surface. These findings demonstrate that the lithium-deficient phases of LN films are effective in facilitating the fabrication of highly doped, crack-free LN films with a variety of dopant elements.

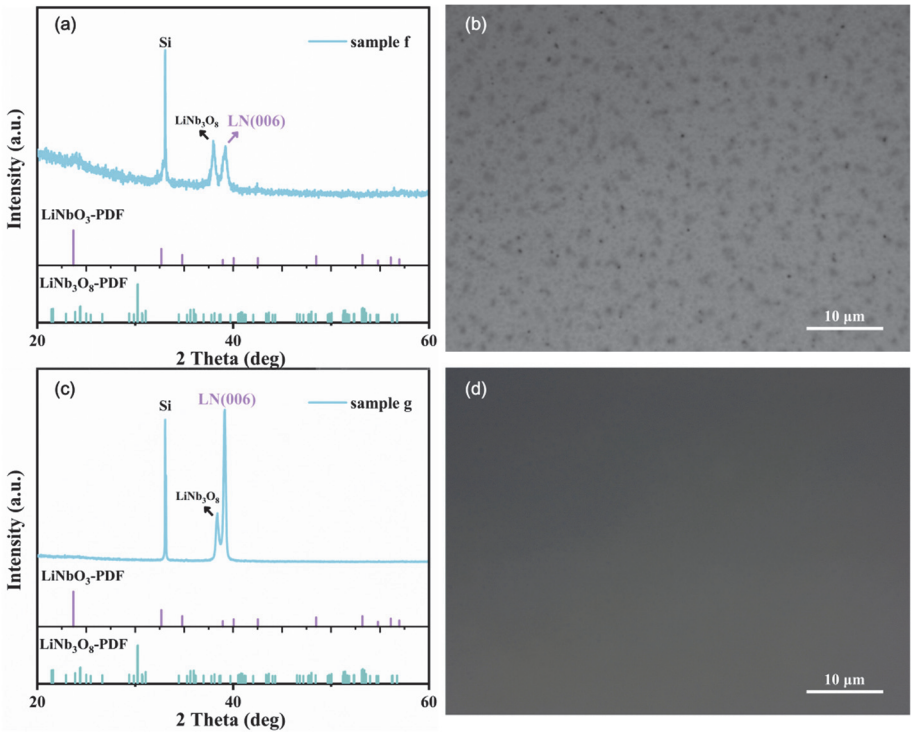


Figure 2. XRD patterns of (**a**) sample f and (**c**) sample g in the 2θ range of 20–60°, compared with reference diffraction patterns of $LiNbO_3$ (ICDD PDF #20-0631) and $LiNb_3O_8$ (ICDD PDF #36-0307); optical micrograph of (**b**) sample f and (**d**) sample g.

3.2. Effect of Lithium-Deficient Phase on Crack-Free LN Films

To further investigate the impact of lithium-deficient phases on the cracking behavior of LN film, samples g–i were deposited on Si <100> substrates at various temperatures. Figure 3a presents the XRD patterns of samples g–i with a magnified view of the <006> diffraction peak region shown in Figure 3b. At the lower deposition temperature of 600 °C, sample i exhibits multiple diffraction peaks corresponding to the <012>, <104>, <006>, <116>, and <018> orientations of $LiNbO_3$. As the deposition temperature increased, the intensity of the <006> peak gradually increased, signifying preferred orientation along the c-axis. The progressive shift in the <006> peak position suggests substantial variations in the unit cell parameters, likely due to enhanced stress arising from increased thermal expansion mismatch between the film and substrate. At a deposition temperature of 750 °C, sample g showed a strong <006> orientation and the presence of a lithium-deficient phase, which is attributed to significant lithium volatilization at elevated temperatures. $LiNb_3O_8$ and $LiNbO_3$ crystallize in different space groups—P21/c and R3c, respectively—as schematically illustrated in Figure 3c,d.

Figure 4a–c present the surface morphologies of samples g–i over a 50 μm × 50 μm area. Sample i exhibited an island-like granular structure, while sample g demonstrated a relatively smooth surface. The root mean square (RMS) roughness decreased markedly from 9.364 nm to 2.036 nm with increasing deposition temperature, indicating enhanced surface flatness and improved film uniformity at elevated temperatures. To further investigate crack formation, surface morphology of the LN film was examined using SEM.

As shown in Figure 4f, cracks are evident on the surface of sample i. With increasing deposition temperature, fine rod-like particles became more pronounced and were observed to accumulate along grain boundaries. Concurrently, the extent of cracking was significantly reduced. Based on the XRD analysis, these rod-like features can be attributed to the formation of lithium-deficient phases.

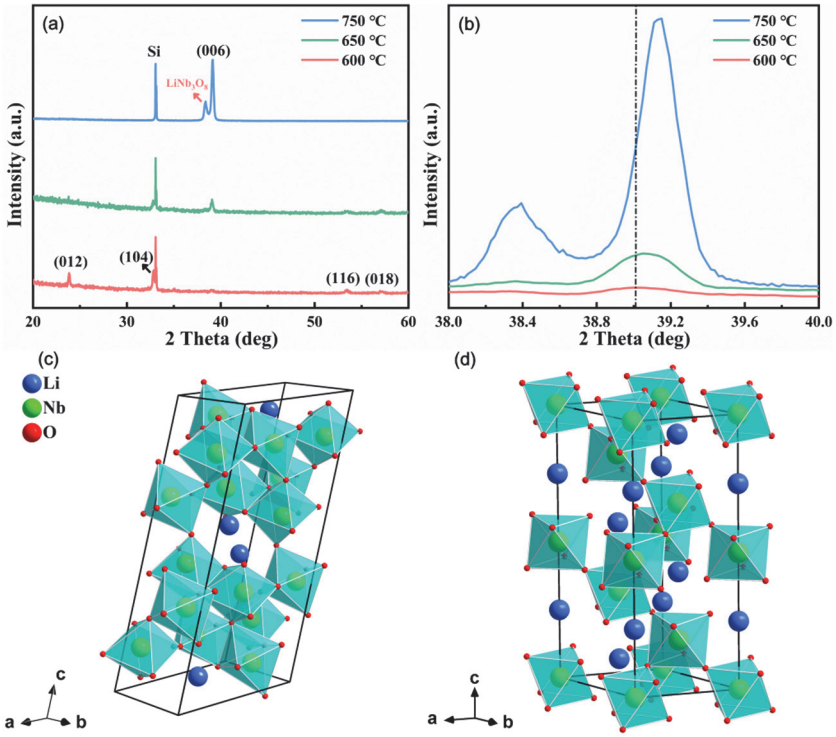


Figure 3. (**a**) XRD patterns and (**b**) enlarged views of the diffraction peaks located at about 39°of LN films were deposited on Si <100> substrates at varying temperatures, respectively; schematic diagram of the structure of (**c**) $LiNb_3O_8$ and (**d**) $LiNbO_3$.

Using Bragg equation, $2d \sin\theta = n\lambda$, along with the 2θ value of the diffraction peak, the out-of-plane lattice parameter (c) of sample h was calculated to be 13.812 Å. This value is slightly smaller than that of the corresponding LN powder (13.860 Å). At this temperature, the deformation of the c-parameter ε_{zz} for the LN film is determined to be 0.35%. The biaxial in-plane stress can be further estimated using Equation (1) [34]:

$$\sigma_b = -\left(\frac{(C_{11}+C_{12})C_{33}}{2C_{13}} + C_{13}\right)\varepsilon_{zz}, \quad (1)$$

where C_{11}, C_{12}, C_{13}, and C_{33} are the stiffness moduli (for congruent LN: C_{11} = 203 GPa, C_{12} = 53 GPa, C_{13} = 75 GPa, and C_{33} = 245 GPa) [35]. The in-plane tensile biaxial stress of sample h is calculated to be 1.2 ± 0.1 GPa.

Due to two primary factors, sample g remains crack-free despite the presence of substantial residual stress. First, films deposited at elevated temperatures exhibit improved crystalline quality, which enhances their mechanical robustness. Second, the lithium-deficient phase inhibits cracking through strain relaxation mechanisms. During the cooling process, thermal stresses—arising from the pronounced mismatch in the coefficients of thermal expansion between lithium niobate and silicon—are typically released at grain boundaries, often resulting in cracking. At higher deposition temperatures, Li_2O preferentially segregates to the film surface and grain boundaries, where it reacts to form the

lithium-deficient phase $LiNb_3O_8$ [36]. The formation of lithium-deficient phase facilitates stress relaxation, thereby enabling the crack-free growth of LN film on silicon substrates.

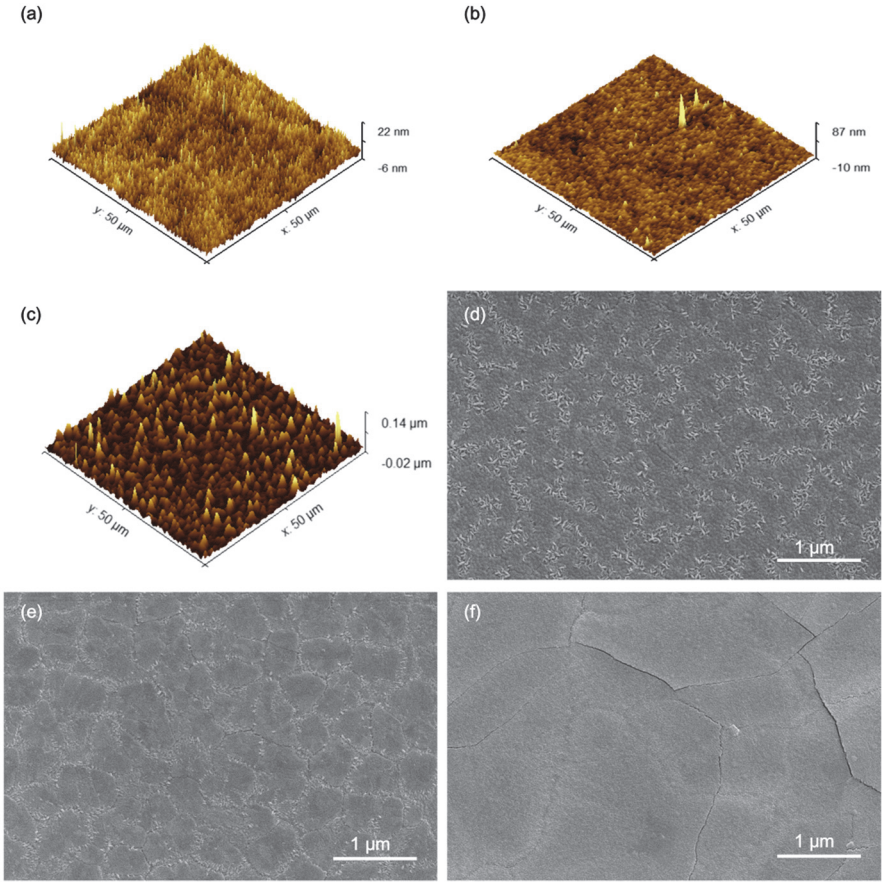


Figure 4. (**a**–**c**) Atomic force microscopy (AFM) topography images of (**a**) sample g, (**b**) sample h, and (**c**) sample i; (**d**–**f**) SEM micrographs of (**d**) sample g, (**e**) sample h, and (**f**) sample i.

3.3. Electrical Properties of Crack-Free LN Films

To further evaluate the potential application of these crack-free LN films, the electrical properties of the films were systematically characterized and analyzed. Figure 5a presents the out-of-plane (OP) PFM phase image of a 17 × 17 µm region obtained from an LN film deposited at 750 °C. These results were obtained following tip-bias polarization of +25 V over a 12 × 12 µm region and subsequent tip-bias polarization of −25 V over the central 5 × 5 µm region. The bright regions in the OP phase image correspond to upward polarization, while the dark regions represent downward polarization. As shown in Figure 5a, the distinct contrast between the bright and dark regions of the two domain states confirms that the sample exhibits clearly switchable polarization properties. Small black regions embedded within the bright and dark domains are distributed throughout the entire scanning area, which can be attributed to the limiting effect of the nonpolar lithium-deficient phases on the switching of ferroelectric domains.

Figure 5b displays the hysteresis loop measurements obtained by scanning an axial direct current (DC) bias from −20 V to +20 V. For LN films deposited at 750 °C, butterfly-shaped amplitude loops and phase hysteresis loops are observed, demonstrating ferroelectric polarization switching and piezoresponse properties. Furthermore, a phase difference of nearly 180° is observed between the upward and downward polarization states, which aligns with the reported characteristics of lithium niobate crystals [37]. *I-U* curves were measured for LN films deposited at 750 °C and 600 °C, as shown in Figure 5c. The Fe-

doped LN films deposited on p-type Si exhibited distinct p-n junction rectification behavior. The uncracked LN films deposited at 750 °C achieved current levels on the order of milliamperes at an applied voltage of 10 V, which is significantly higher than the currents observed for the cracked LN films deposited at 600 °C. The apparent conductivities of the LN films deposited at 750 °C and 600 °C under a 10 V applied voltage were measured to be 9.95×10^{-5} S/m and 5.93×10^{-7} S/m, respectively.

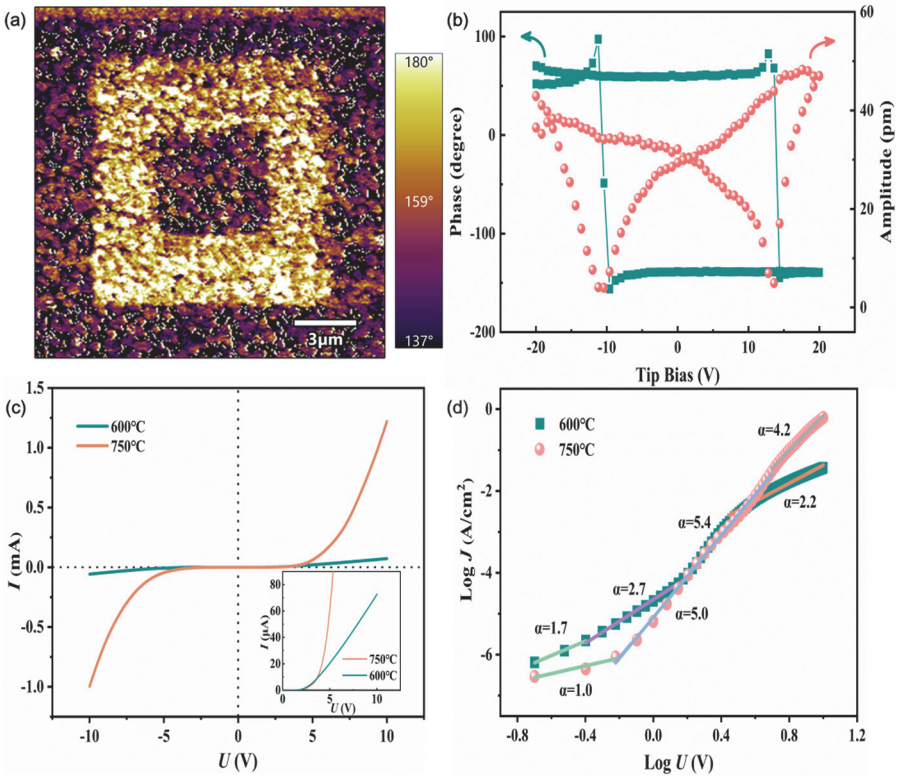


Figure 5. (**a**) Out-of-plane (OP) phase image obtained via piezoresponse force microscopy (PFM) and (**b**) local PFM hysteresis loops depicting both the phase and amplitude signals of sample g. (**c**) The current-voltage (*I*-*U*) characteristics and (**d**) the log*J*–log*U* curves of the LN films at various deposition temperatures (the inset in (**c**) presents a magnified view of the *I*-*U* curve in the range of 0 to +10 V).

The log*J*–log*U* curves for samples deposited at different temperatures are presented in Figure 5d, and the slope (α) was calculated through linear fitting. The linear fitting results for all LN films align with space-charge-limited current (SCLC) theory [38]. At low voltage, the phase with a slope of $\alpha = 1$ corresponds to the ohmic conduction mechanism, which is governed by electronic excitation. As the voltage increases, the conduction mechanism transitions to a trap-filling limited (TFL) mechanism, dominated by the filling of traps. Once the traps are fully filled, the slope (α) stabilizes at approximately 2. At this stage, the conduction mechanism of the thin film aligns with the Mott–Gurney law, where the conduction current can be described by the following Equation (2) [39]:

$$J = \frac{9\mu_p \varepsilon_r \varepsilon_0 U^2}{8d^2}, \quad (2)$$

where μ_p is the charge carrier mobility, ε_r is the relative dielectric constant, ε_0 is the vacuum dielectric constant, U is the bias voltage, and d is the thickness of the sample. The LN films deposited at 750 °C have not achieved complete trap filling at 10 V, likely due to the formation of the lithium-deficient phase $LiNb_3O_8$. This lithium-deficient phase not only

mitigates macroscopic cracking in films but also enables them to achieve a conductivity two orders of magnitude higher than that of cracked single-phase LN films.

4. Conclusions

We have successfully fabricated a series of LN films via PLD, achieving high doping concentrations of 5.0% for both Er^{3+} and Fe^{3+}. By introducing a lithium-deficient phase, crack-free, highly doped LN films on silicon substrates were obtained. The presence of a lithium-deficient phase plays a critical role in alleviating crack formation during LN film growth. The Fe^{3+}-enriched, crack-free LN films exhibit not only distinct polarization switching behavior but also significantly enhanced electrical conductivity of 9.95×10^{-5} S/m. This effectively addresses the intrinsic limitations of conventional lithium niobate in optoelectronic applications, offering promising prospects for expanding the functional landscape of lithium niobate in photodetection and other advanced optoelectronic applications. In the next phase of this work, we will further investigate the growth conditions to achieve crack-free silicon-based LN films.

Author Contributions: Formal analysis, S.S. and T.X.; investigation, S.S. and T.X.; data curation, S.S. and T.X.; writing—original draft preparation, S.S. and T.X.; writing—review and editing, J.S., H.L., D.Z. and Y.K.; supervision, H.L., D.Z., Y.K. and J.X.; funding acquisition, Y.K. and J.X. All authors have read and agreed to the published version of the manuscript.

Funding: This work was supported by the National Natural Science Foundation of China (12034010, 12134007, 12474386), the National Key Research and Development Program of China (2019YFA0705000), the Natural Science Foundation of Tianjin (23JCZDJC00780), and the Program for Changjiang Scholars and Innovative Research Team in University (IRT_13R29).

Institutional Review Board Statement: Not applicable.

Informed Consent Statement: Not applicable.

Data Availability Statement: The data that support the findings of this study are available from the corresponding authors upon reasonable request.

Conflicts of Interest: The authors declare no conflicts of interest.

References

1. Boes, A.; Corcoran, B.; Chang, L.; Bowers, J.; Mitchell, A. Status and Potential of Lithium Niobate on Insulator (LNOI) for Photonic Integrated Circuits. *Laser Photon. Rev.* **2018**, *12*, 1700256. [CrossRef]
2. Boes, A.; Chang, L.; Langrock, C.; Yu, M.; Zhang, M.; Lin, Q.; Lončar, M.; Fejer, M.; Bowers, J.; Mitchell, A. Lithium niobate photonics: Unlocking the electromagnetic spectrum. *Science* **2023**, *379*, eabj4396. [CrossRef]
3. Xie, H.; Yang, T.; Wei, Y.; Guan, H.; Lu, H. Recent Research Progress of Thin film Lithium Niobate Photodetector. *J. Synth. Cryst.* **2024**, *53*, 410–425. [CrossRef]
4. Xu, X.; Wang, T.; Chen, P.; Zhou, C.; Ma, J.; Wei, D.; Wang, H.; Niu, B.; Fang, X.; Wu, D.; et al. Femtosecond laser writing of lithium niobate ferroelectric nanodomains. *Nature* **2022**, *609*, 496–501. [CrossRef] [PubMed]
5. Kong, Y.; Bo, F.; Wang, W.; Zheng, D.; Liu, H.; Zhang, G.; Rupp, R.; Xu, J. Recent Progress in Lithium Niobate: Optical Damage, Defect Simulation, and On-Chip Devices. *Adv. Mater.* **2020**, *32*, 1806452. [CrossRef] [PubMed]
6. Xu, Y.; Sayem, A.A.; Fan, L.; Zou, C.L.; Wang, S.; Cheng, R.; Fu, W.; Yang, L.; Xu, M.; Tang, H.X. Bidirectional interconversion of microwave and light with thin-film lithium niobate. *Nat. Commun.* **2021**, *12*, 4453. [CrossRef] [PubMed]
7. Lin, J.; Gao, R.; Guan, J.; Li, C.; Yao, N.; Cheng, Y. Advances in Low-Loss Thin-Film Lithium Niobate Photonic Integrated Devices. *J. Synth. Cryst.* **2024**, *53*, 372–394. [CrossRef]
8. Jia, Y.; Wang, L.; Chen, F. Ion-cut lithium niobate on insulator technology: Recent advances and perspectives. *Appl. Phys. Rev.* **2021**, *8*, 011307. [CrossRef]
9. Zhuang, R.; He, J.; Qi, Y.; Li, Y. High-Q Thin-Film Lithium Niobate Microrings Fabricated with Wet Etching. *Adv. Mater.* **2023**, *35*, 2208113. [CrossRef]
10. Wang, C.; Zhang, M.; Chen, X.; Bertrand, M.; Shams-Ansari, A.; Chandrasekhar, S.; Winzer, P.; Lončar, M. Integrated lithium niobate electro-optic modulators operating at CMOS-compatible voltages. *Nature* **2018**, *562*, 101–104. [CrossRef]

11. Snigirev, V.; Riedhauser, A.; Lihachev, G.; Churaev, M.; Riemensberger, J.; Wang, R.N.; Siddharth, A.; Huang, G.; Möhl, C.; Popoff, Y.; et al. Ultrafast tunable lasers using lithium niobate integrated photonics. *Nature* **2023**, *615*, 411–417. [CrossRef]
12. Yu, Z.; Sun, X. Acousto-optic modulation of photonic bound state in the continuum. *Light Sci. Appl.* **2020**, *9*, 1. [CrossRef]
13. Wan, L.; Yang, Z.; Zhou, W.; Wen, M.; Feng, T.; Zeng, S.; Liu, D.; Li, H.; Pan, J.; Zhu, N.; et al. Highly efficient acousto-optic modulation using nonsuspended thin-film lithium niobate-chalcogenide hybrid waveguides. *Light Sci. Appl.* **2022**, *11*, 145. [CrossRef]
14. Zhang, M.; Buscaino, B.; Wang, C.; Shams-Ansari, A.; Reimer, C.; Zhu, R.; Kahn, J.M.; Lončar, M. Broadband electro-optic frequency comb generation in a lithium niobate microring resonator. *Nature* **2019**, *568*, 373–377. [CrossRef]
15. Zhang, K.; Sun, W.; Chen, Y.; Feng, H.; Zhang, Y.; Chen, Z.; Wang, C. A power-efficient integrated lithium niobate electro-optic comb generator. *Commun. Phys.* **2023**, *6*, 17. [CrossRef]
16. Wang, C.; Langrock, C.; Marandi, A.; Jankowski, M.; Zhang, M.; Desiatov, B.; Fejer, M.M.; Lončar, M. Ultrahigh-efficiency wavelength conversion in nanophotonic periodically poled lithium niobate waveguides. *Optica* **2018**, *5*, 1438–1441. [CrossRef]
17. Lu, J.; Surya, J.B.; Liu, X.; Bruch, A.W.; Gong, Z.; Xu, Y.; Tang, H.X. Periodically poled thin-film lithium niobate microring resonators with a second-harmonic generation efficiency of 250,000%/W. *Optica* **2019**, *6*, 1455–1460. [CrossRef]
18. Ma, Z.; Chen, J.Y.; Li, Z.; Tang, C.; Sua, Y.M.; Fan, H.; Huang, Y.P. Ultrabright Quantum Photon Sources on Chip. *Phys. Rev. Lett.* **2020**, *125*, 263602. [CrossRef] [PubMed]
19. Zhao, J.; Ma, C.; Rüsing, M.; Mookherjea, S. High Quality Entangled Photon Pair Generation in Periodically Poled Thin-Film Lithium Niobate Waveguides. *Phys. Rev. Lett.* **2020**, *124*, 163603. [CrossRef] [PubMed]
20. Ruan, Z.; Chen, K.; Wang, Z.; Fan, X.; Gan, R.; Qi, L.; Xie, Y.; Guo, C.; Yang, Z.; Cui, N.; et al. High-Performance Electro-Optic Modulator on Silicon Nitride Platform with Heterogeneous Integration of Lithium Niobate. *Laser Photon. Rev.* **2023**, *17*, 2200327. [CrossRef]
21. Zhou, Y.; Zhu, Y.; Fang, Z.; Yu, S.; Huang, T.; Zhou, J.; Wu, R.; Liu, J.; Ma, Y.; Wang, Z.; et al. Monolithically Integrated Active Passive Waveguide Array Fabricated on Thin Film Lithium Niobate Using a Single Continuous Photolithography Process. *Laser Photon. Rev.* **2023**, *17*, 2200686. [CrossRef]
22. Chen, K.; Zhu, Y.; Liu, Z.; Xue, D. State of the Art in Crystallization of $LiNbO_3$ and Their Applications. *Molecules* **2021**, *26*, 7044. [CrossRef]
23. Ogugua, S.N.; Ntwaeaborwa, O.M.; Swart, H.C. Latest Development on Pulsed Laser Deposited Thin Films for Advanced Luminescence Applications. *Coatings* **2020**, *10*, 1078. [CrossRef]
24. Paldi, R.L.; Qi, Z.; Misra, S.; Lu, J.; Sun, X.; Phuah, X.L.; Kalaswad, M.; Bischoff, J.; Branch, D.W.; Siddiqui, A.; et al. Nanocomposite-Seeded Epitaxial Growth of Single-Domain Lithium Niobate Thin Films for Surface Acoustic Wave Devices. *Adv. Photon. Res.* **2021**, *2*, 2000149. [CrossRef]
25. Li, W.; Cui, J.; Wang, W.; Zheng, D.; Jia, L.; Saeed, S.; Liu, H.; Rupp, R.; Kong, Y.; Xu, J. P-Type Lithium Niobate Thin Films Fabricated by Nitrogen-Doping. *Materials* **2019**, *12*, 819. [CrossRef]
26. Sauze, L.C.; Vaxelaire, N.; Templier, R.; Rouchon, D.; Pierre, F.; Guedj, C.; Remiens, D.; Rodriguez, G.; Bousquet, M.; Dupont, F.; et al. Homo-epitaxial growth of $LiNbO_3$ thin films by Pulsed Laser deposition. *J. Cryst. Growth* **2023**, *601*, 126950. [CrossRef]
27. Fakhri, M.A.; Alwahib, A.A.; Alhasan, S.F.H.; Salim, E.T.; Ibrahim, R.K.; Alsultany, F.H.; Abdulwahab, A.W.; Hashim, U. Optoelectronic device based on lithium niobate nanofilms deposited at various pulsed laser wavelengths. *J. Opt.* **2023**, *52*, 2356–2365. [CrossRef]
28. Bo, F.; Wang, J.; Cui, J.; Ozdemir, S.K.; Kong, Y.; Zhang, G.; Xu, J.; Yang, L. Lithium-Niobate–Silica Hybrid Whispering-Gallery-Mode Resonators. *Adv. Mater.* **2015**, *27*, 8075–8081. [CrossRef]
29. Bartasyte, A.; Margueron, S.; Baron, T.; Oliveri, S.; Boulet, P. Toward High-Quality Epitaxial $LiNbO_3$ and $LiTaO_3$ Thin Films for Acoustic and Optical Applications. *Adv. Mater. Interfaces* **2017**, *4*, 1600998. [CrossRef]
30. Tada, H.; Kumpel, A.E.; Lathrop, R.E.; Slanina, J.B.; Nieva, P.; Zavracky, P.; Miaoulis, I.N.; Wong, P.Y. Thermal expansion coefficient of polycrystalline silicon and silicon dioxide thin films at high temperatures. *J. Appl. Phys.* **2000**, *87*, 4189. [CrossRef]
31. Wang, S.J.; Panhans, M.; Lashkov, I.; Kleemann, H.; Caglieris, F.; Becker-Koch, D.; Vahland, J.; Guo, E.; Huang, S.; Krupskaya, Y.; et al. Highly efficient modulation doping: A path toward superior organic thermoelectric devices. *Sci. Adv.* **2022**, *8*, eabl9264. [CrossRef] [PubMed]
32. Chen, R.; Li, Y.C.; Cai, J.M.; Cao, K.; Lee, H.B.R. Atomic level deposition to extend Moore's law and beyond. *Int. J. Extrem. Manuf.* **2020**, *2*, 022002. [CrossRef]
33. Huang, Z.; Shao, G.; Li, L. Micro/nano functional devices fabricated by additive manufacturing. *Prog. Mater. Sci* **2023**, *131*, 101020. [CrossRef]
34. Bartasyte, A.; Plausinaitiene, V.; Abrutis, A.; Murauskas, T.; Boulet, P.; Margueron, S.; Gleize, J.; Robert, S.; Kubilius, V.; Saltyte, Z. Residual stresses and clamped thermal expansion in $LiNbO_3$ and $LiTaO_3$ thin films. *Appl. Phys. Lett.* **2012**, *101*, 122902. [CrossRef]
35. Warner, A.W.; Onoe, M.; Coquin, G.A. Determination of Elastic and Piezoelectric Constants for Crystals in Class (3m). *J. Acoust. Soc. Am.* **1967**, *42*, 1223–1231. [CrossRef]

36. Akazawa, H.; Shimada, M. Mechanism for $LiNb_3O_8$ phase formation during thermal annealing of crystalline and amorphous $LiNbO_3$ thin films. *J. Mater. Res.* **2007**, *22*, 1726–1736. [CrossRef]
37. Gonnissen, J.; Batuk, D.; Nataf, G.F.; Jones, L.; Abakumov, A.M.; Van Aert, S.; Schryvers, D.; Salje, E.K. Direct Observation of Ferroelectric Domain Walls in $LiNbO_3$: Wall-Meanders, Kinks, and Local Electric Charges. *Adv. Funct. Mater.* **2016**, *26*, 7599–7604. [CrossRef]
38. Xiao, Z.; Xiao, T.; Wang, S.; Huang, S.; Wei, B.; Liu, W. The novel electrical properties in quasi-2D hybrid improper ferroelectric $Sr_3Sn_2O_7$ ceramic and the structural modulation. *J. Am. Ceram. Soc.* **2024**, *107*, 334–343. [CrossRef]
39. Chandra, W.; Ang, L.K.; Pey, K.L.; Ng, C.M. Two-dimensional analytical Mott-Gurney law for a trap-filled solid. *Appl. Phys. Lett.* **2007**, *90*, 153505. [CrossRef]

Disclaimer/Publisher's Note: The statements, opinions and data contained in all publications are solely those of the individual author(s) and contributor(s) and not of MDPI and/or the editor(s). MDPI and/or the editor(s) disclaim responsibility for any injury to people or property resulting from any ideas, methods, instructions or products referred to in the content.